SYNTHESIS, CRYSTALLINE STRUCTURE, ANALYSIS OF DIHALIDE BIS ((PYRIDIN-1-IUM-4-YL) METHANAMINIUM) HEXAGALOSTANNATE (IV).

P. K. Kodamboev
Khorezm Mamun branch of Uzbekistan Academy of Sciences, Markaz-1, Khiva 220900, Uzbekistan.
Kh. Kh. Turaev
Termez state University 190111, 43 Barkamol Avlod Street, Termez, Uzbekistan.
A. B. Ibragimov
Institute of General and Inorganic Chemistry of Uzbekistan Academy of Sciences, 100170, Mirzo Ulug'bek str., 77a Tashkent, Uzbekistan.
C. Balakrishnan
Institute of General and Inorganic Chemistry of Uzbekistan Academy of Sciences, 100170, Mirzo Ulug'bek str., 77a Tashkent, Uzbekistan.
F. S. Narimanova
Termez state University 190111, 43 Barkamol Avlod Street, Termez, Uzbekistan.
F. Z. Gulomov
Westminster International University in Tashkent

Annotatsiya: Yangi sintez qilingan organik-noorganik gibridlarning monokristallari, ya'ni bis ((piridin-1-ium-4-il) metanaminiy) geksaxalostannat (IV) dixlorid (1) va bis ((piridin-1-ium-4-il) metanaminiy) geksaxalostannat (IV) dibromid (2) monokristallari muvaffaqiyatli o'stirilgan va keyinchalik monokristall rentgenografik tahlil yordamida batafsil tavsiflangan. Eksperimental rentgenogrammalar o'tkir va yuqori intensivlikdagi cho'qqilarni namoyon qiladi, bu sintez qilingan komplekslarning yuqori kristalliligi va strukturaviy yaxlitligini tasdiqlaydi. Gibrid materiallarning taqiqlangan zona oraliqlarini galoid ionini o'zgartirish orqali samarali sozlash mumkin, bu birikma (1) uchun 4,21 eV va birikma (2) uchun 2,93 eV taqiqlangan zona oraliqlari bilan tasdiqlanadi. Fotolyuminessensiya tadqiqotlari shuni ko'rsatadiki, ikkala birikma ham xona haroratida qattiq holatda fluoressensiya chiqaradi. Bundan tashqari, bog'larning valentlik yig'indisini hisoblash natijasida qalayning +4 formal oksidlanish darajasiga ega ekanligi tasdiqlandi. Molekulalararo o'zaro ta'sirlarni va kristall to'plamlarni o'rganish

Kalit so'zlar: Organik-noorganik gibrid; Kristall strukturasi; Xirshfeld yuzasi; Z-skaner tadqiqotlari; valent bog'lanish; Bog'larning valentlik yig'indisi

Аннотация: Монокристаллы вновь синтезированных органико-неорганических гибридов, а именно бис ((пиридин-1-иум-4-ил)

ISSN 3030-3907

метанаминий) гексахалостаннат (IV) дихлорид (1) и бис ((пиридин-1-иум-4-ил) метанаминий) гексахалостаннат (IV) дибромид (2), были успешно выращены и впоследствии подвергнуты детальной характеристике с использованием монокристаллического рентгеноструктурного анализа. Экспериментальные рентгеноструктурные схемы демонстрируют резкие и высокоинтенсивные пики, свидетельствующие о высокой кристалличности и структурной целостности синтезированных комплексов. Полосовые разрывы гибридных материалов можно эффективно регулировать, изменяя галогенид-ион, о чем свидетельствуют различные полосовые разрывы 4,21 эВ для соединения (1) и 2,93 эВ для соединения (2). Фотолюминесцентные исследования показывают, что оба соединения испускают флуоресценцию в твердом состоянии при комнатной температуре. Кроме того, расчеты суммы валентностей связей подтвердили, что олово обладает формальной степенью окисления +4. Изучение межмолекулярных взаимодействий и кристаллической упаковки

Ключевые слова: Органические и неорганические гибриды; Кристаллическая структура; поверхность Хиршфельда; Z-сканирование исследований; полосовой зазор; Валентная сумма связей

Abstract: Single crystals of the newly synthesized organic-inorganic hybrids, namely bis((pyridin-1-ium-4-yl)methanaminium) hexahalostannate(IV) dichloride (1) and bis((pyridin-1-ium-4-yl)methanaminium) hexahalostannate(IV) dibromide (2), were successfully grown and subsequently subjected to detailed characterization using single-crystal X-ray diffraction analysis. The experimental XRD patterns exhibit sharp and high-intensity peaks, attesting to the high crystallinity and structural integrity of the synthesized complexes. The band gaps of the hybrid materials can be effectively tuned by altering the halide ion, as evidenced by the different band gaps of 4.21 eV for compound (1) and 2.93 eV for compound (2). Photoluminescence investigations reveal that both compounds emit fluorescence in the solid state at room temperature. Additionally, bond valence sum calculations have verified that tin possesses a formal oxidation state of +4. Examination of intermolecular interactions and crystal packing through Hirshfeld surface analysis.

Keywords: Organic-inorganic hybrids; Crystal structure; Hirshfeld surface; Z-scan studies; Band gap; Bond valence sum

1. Introduction

In recent years, synthetic perovskites composed of organic-inorganic hybrid materials have emerged as a vibrant area of research, capturing the attention of scientists and engineers alike [1-3]. These hybrid materials, often referred to as organic-inorganic perovskites, exhibit a rich tapestry of structural, electrical,

ISSN 3030-3907

optical, and thermal properties, making them highly attractive for a wide range of applications [4-8]. The unique combination of organic and inorganic components within these materials introduces a level of versatility and tunability that is unparalleled in traditional inorganic perovskite structures [9-11]. This hybrid nature allows for precise control over the composition, morphology, and properties of the resulting materials, paving the way for tailored functionalities to suit specific application requirements. From a structural standpoint, organic-inorganic perovskites often exhibit intriguing arrangements at the atomic and molecular levels, leading to diverse crystal structures and bonding motifs [12]. These structural nuances not only contribute to the materials' fundamental properties but also offer insights into their synthesis, stability, and performance. Furthermore, the electrical properties of these materials have garnered significant interest due to their potential applications in electronic and optoelectronic devices [13-15]. By carefully engineering the composition and morphology of organic-inorganic perovskites, researchers can achieve desirable charge transport characteristics, opening up avenues for high-performance transistors, photodetectors, solar cells and nonlinear optical (NLO) materials [16-20].

In this study, a detailed examination encompassing structural characterization and optical properties of the intriguing hybrid perovskites bis((pyridin-1-ium-4-yl)methanaminium) hexahalostannate(IV) dichloride (1) and bis((pyridin-1-ium-4-yl)methanaminium) hexahalostannate(IV) dibromide (2) was conducted. To elucidate molecular interactions within these materials, we employ advanced analytical techniques, including the generation of fingerprint plots derived from Hirshfeld surfaces. This multifaceted investigation not only sheds light on the structural and optical characteristics of the studied perovskites but also provides valuable insights into their underlying molecular arrangements and intermolecular interactions.

2. Experimental

2.1 Synthesis and crystal growth

Synthesis of bis((pyridin-1-ium-4-yl)methanaminium) hexahalostannate(IV) dichloride (1)

A precursor solution of (pyridin-1-ium-4-yl)methanaminium dichloride was prepared by mixing 4-pyridinemethanamine (1.10 g, 10 mM) and HCl (1 mL) in diethyl ether (10 mL) at room temperature. The mixture was then heated to 60°C for 10 minutes. Upon cooling, the (pyridin-1-ium-4-yl)methanaminium dichloride precipitated from the solution and was isolated by washing with diethyl ether before being dissolved in ethanol. Tin chloride was prepared by dissolving tin shots (0.118 g, 5 mM) in 5 mL of 36% hydrochloric acid at room temperature for 7 h.This tin chloride solution was then added to the ethanolic solution of the (pyridin-1-ium-

ISSN 3030-3907

4-yl)methanaminium dichloride precursor with continuous stirring according to Scheme 1. Crystals formed from the solution after 15-17 d, yielding 82%, dec.: 242-245°C. Elemental analysis: %, Anal. Calcd. for $C_{12}H_{20}N_4Cl_8Sn$ (622.63 g/mole): C, 23.15; H, 3.215; N, 9.0. Found (%) C, 22.81; H, 3.21; N, 8.89.

Synthesis of bis((pyridin-1-ium-4-yl)methanaminium) hexahalostannate(IV) dibromide (2)

A solution of (pyridin-1-ium-4-yl)methanaminium dibromide precursor was synthesized by mixing 4-pyridinemethanamine (1.10 g, 10 mM) and hydrobromic acid (1 mL) in diethyl ether (10 mL) at room temperature. The mixture was heated at 60°C for 10 minutes, resulting in the precipitation of (pyridin-1-ium-4-yl)methanaminium dibromide upon cooling. The precipitate was washed with diethyl ether and dissolved in ethanol. In parallel, tin bromide was prepared by dissolving tin shots (0.118 g, 5 mM) in 5 mL hydrobromic acid (48%) at room temperature for seven hours. The tin chloride solution was then added to the freshly prepared ethanolic solution of (pyridin-1-ium-4-yl)methanaminium dibromide precursor with continuous stirring as per Scheme 1. Crystallization occurred after 15-17 d, yielding 82%, dec.: 263-264°C. Elemental analysis: % Anal. Calcd. for $C_{12}H_{20}N_4Br_8Sn$ (978.29 g/mole): C, 14.72; H, 2.0; N, 5.724. Found (%): C, 14.59; H, 1.97; N, 5.708.

2.2. Characterization techniques

FT-IR spectra were obtained using a Shimadzu IR Affinity-1 spectrophotometer with KBr discs, while elemental analysis of the compounds was performed using the Dumas method on an ELEMENTARY UNICUBE® IZI (CHNS/O) analyzer. NMR spectra were recorded at room temperature using a 400 MHz Bruker AMX-400 spectrometer. For ^{1}H and ^{13}C NMR, compounds (1) and (2) were dissolved in DMSO-d6 with TMS as the internal standard.The Shimadzu UV3600 UV-Vis spectrophotometer and the Jobin Yvon Fluorolog-FL3-11 spectrofluorometer were used to record the UV-DRS and photoluminescence spectra, respectively. The X-ray fluorescence (XRF) spectra were recorded by Epsilon4 hardware (in Epsilon3 software package) with Omnian automatic standard (He 0.61L/min). An Ultima-IV, Rigaku X-ray diffractometer (CuKα radiation, λ = 1.5406 Å) was used to record powder X-ray diffraction patterns. An Oxford Diffraction Xcalibur-R CCD diffractometer was used for collecting data for the crystal structure determinations. The computer programs SHELXS-97 and **2.2. Characterization Techniques

Fourier-transform infrared (FT-IR) spectra were acquired in the range of 400–4000 cm^{-1} using a Shimadzu IR Affinity-1 spectrophotometer (Shimadzu Corporation, Kyoto, Japan). Samples were prepared as transparent pellets by thoroughly grinding approximately 1–2 mg of the finely powdered compound with

ISSN 3030-3907

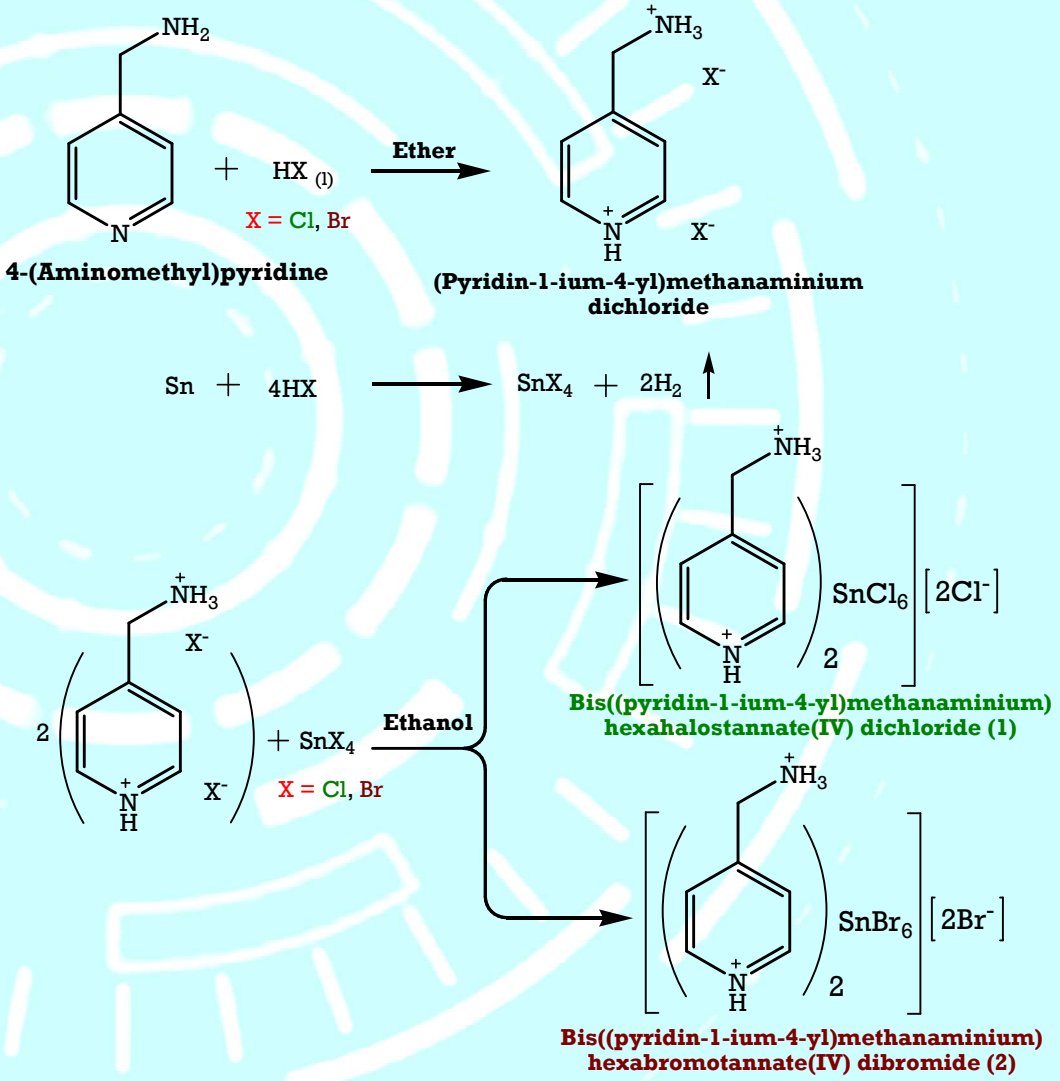
100–200 mg of spectroscopic-grade potassium bromide (KBr) and pressing the mixture under high pressure (ca. 10 tons) in a hydraulic press to form thin, uniform discs.

Elemental analysis for carbon, hydrogen, nitrogen, sulfur, and oxygen (CHNS/O) content was carried out using the Dumas combustion method on an ELEMENTARY UNICUBE® IZI elemental analyzer (Elementar Analysensysteme GmbH, Langenselbold, Germany). Accurately weighed samples (2–3 mg) were combusted at 1150 °C in a helium/oxygen atmosphere, and the resulting gases were separated and quantified via thermal conductivity detection (TCD). All measurements were performed in triplicate to ensure reproducibility, with deviations typically within ±0.4% of the theoretical values. ^{1}H and ^{13}C nuclear magnetic resonance (NMR) spectra were recorded at ambient temperature (298 K) on a Bruker AMX-400 spectrometer (Bruker BioSpin GmbH, Rheinstetten, Germany) operating at 400.13 MHz for ^{1}H and 100.61 MHz for ^{13}C. Compounds (1) and (2) were dissolved in deuterated dimethyl sulfoxide (DMSO-d_6, 99.9% D, containing 0.03% v/v TMS) to prepare solutions of approximately 10–15 mg/mL for ^{1}H NMR and 30–40 mg/mL for ^{13}C NMR. Tetramethylsilane (TMS) was used as the internal chemical shift reference (δ = 0.00 ppm). Standard pulse sequences were employed: ^{1}H NMR (zg30, 32 scans, relaxation delay 1.0 s), ^{13}C NMR (zgpg30, 1024–4096 scans, relaxation delay 2.0 s). All spectra were processed using Bruker TopSpin 3.6 software with automatic baseline correction and phase adjustment.

UV-Vis diffuse reflectance spectra (UV-DRS) were measured in the wavelength range of 200–800 nm on a Shimadzu UV3600 double-beam spectrophotometer (Shimadzu Corporation, Kyoto, Japan) equipped with an integrating sphere attachment (ISR-603). Barium sulfate ($BaSO_4$) was used as a non-absorbing reflectance standard (100% reflectance). Solid samples were finely ground and evenly spread over the $BaSO_4$ reference layer. The reflectance data were converted to absorbance using the Kubelka–Munk function

Photoluminescence (PL) emission and excitation spectra were recorded at room temperature using a Jobin Yvon Fluorolog-FL3-11 spectrofluorometer (HORIBA Jobin Yvon Inc., Edison, NJ, USA) equipped with a 450 W xenon arc lamp as the excitation source and a double-grating monochromator for both excitation and emission pathways. Solid samples were placed in a front-face sample holder to minimize self-absorption. Emission spectra were typically collected at a fixed excitation wavelength (selected from excitation scans), with slit widths of 2–5 nm and integration times of 0.1–1.0 s. All spectra were corrected for the spectral response of the instrument and the xenon lamp intensity profile.

ISSN 3030-3907



Scheme 1. Synthesis of (1) and (2).

And refined using a riding model. SHELXL-97 were used to solve and refine the structure. Crystal Explorer 3.1 produced fingerprint plots and Hirshfeld surface maps [21].

3. Results and discussion

3.1. Single-crystal X-ray structure analysis

Single crystals of bis((pyridin-1-ium-4-yl)methanaminium) hexahalostannate(IV) dichloride (1) and bis((pyridin-1-ium-4-yl)methanaminium) hexahalostannate(IV) dibromide (2) were precisely obtained for X-ray analysis. This was achieved through the gradual evaporation of ethanolic solutions comprising the reaction mixture, conducted under ambient conditions. The resulting crystals exhibited the requisite structural integrity and purity necessary for detailed X-ray characterization. Table 1 presents comprehensive crystallographic data, including details of data collection refinement parameters, and the outcomes of the analyses conducted on the compounds. Additionally, Tables S1 and S2 contain exhaustive listings of bond lengths, bond angles, and dihedral angles for further structural elucidation. It is noteworthy that both

ISSN 3030-3907

compounds exhibit isostructural characteristics, albeit with minor variances in lattice parameters. Furthermore, their crystalline forms conform to the triclinic crstal system, with a centrosymmetric space group denoted as Pī. Fig. 2 presents the Oak Ridge Thermal-Ellipsoid Plots for the two synthesized compounds, detailing atomic thermal vibrations, molecular geometry, and stability. The ellipsoids illustrate anisotropic displacement parameters, indicating positional uncertainties and thermal motion of the atoms. Fig. S1 illustrates a comparative analysis of the molecular packing arrangements within the unit cell. This figure provides a examination of how the molecules are organized and interact within the crystalline structure.

The asymmetric unit of compound (1) comprises a single diprotonated cation $(C_6H_{10}N_2)^{2+}$, one chloride, and half of a $[SnCl_6]^{2-}$ anion. These components are intricately linked by hydrogen bonds, specifically N-H•••Cl interactions. The cation provides two protons that form strong hydrogen bonds with the chloride ion, facilitating a robust network of intermolecular interactions. This hydrogen bonding not only stabilizes the overall structure but also influences the packing and arrangement of the ions within the crystal lattice. The presence of the $[SnCl_6]^{2-}$ anion, albeit in a symmetric half-occupancy, further contributes to the structural integrity and the three-dimensional architecture of the compound. In the crystal structure, the Sn-Cl bond distances range from 2.4176(5) Å to 2.4398(5) Å, indicating a uniform bonding environment around the tin atom. The Cl-Sn-Cl bond angles vary between 87.73° and 92.27°, reflecting slight deviations from ideal octahedral geometry. The compound exhibits extensive hydrogen-bonding interactions, significantly contributing to its stability and structural organization. The Sn atom is six-coordinated, forming a quasi-regular octahedral arrangement. This coordination geometry is stabilized by the surrounding chloride ions, which, along with the hydrogen bonds, create a robust three-dimensional network within the crystal lattice. The nearly regular octahedral configuration of the $SnCl_6^{2-}$ anion, combined with the extensive hydrogen bonding, highlights the intricate balance of forces that define the structural characteristics of this compound. Table 2 details the polyhedral properties of compound (1), specifically focusing on the $SnCl_6^{2-}$ anion. This anion exhibits octahedral coordination geometry, as illustrated in Fig. S2(a). The bond angle variance is recorded at 2.9569°, indicating very slight deviations from the ideal octahedral angles, which are typically 90°. Additionally, the effective coordination number is calculated to be 5.9972, which is remarkably close to the ideal value of 6. These measurements collectively demonstrate that the $SnCl_6^{2-}$ anion maintains nearly perfect octahedral geometry. The minimal bond angle variance suggests a highly symmetrical and stable coordination environment around the tin atom. This structural integrity is crucial for the overall stability and

ISSN 3030-3907

functionality of the compound. The inter- and intramolecular hydrogen bonds present in compound (1) are detailed in Table 3 and illustrated in Fig. 3(a). Notably, the hydrogen atom H(2A) participates in three-center hydrogen bonding interactions with three chlorine atoms. These interactions include N(2)•••Cl(1), N(2)•••Cl(2), and N(2)•••Cl(3), with corresponding distances of 3.477(4) Å, 3.575(1) Å, and 3.324(2) Å, respectively. This intricate hydrogen bonding network significantly contributes to the stability and structural integrity of the compound. The three-center hydrogen bonding involving the H(2A) atom indicates a complex yet stable interaction pattern, which helps to hold the crystal lattice together. The centroid-centroid contact distance between adjacent aromatic rings is 3.699 Å, with an interplanar angle of 21.58°. This stacking arrangement exhibits the characteristics of slipped stacking alignment. The horizontal displacement of the rings, or the offset, ranges from 1.335 Å to 1.385 Å, while the plane-to-plane distance is measured at 3.403 Å (Fig. 4(a)). This offset stacking arrangement indicates a significant π-π interaction, which contributes to the overall stability and structural cohesion of the crystal lattice.

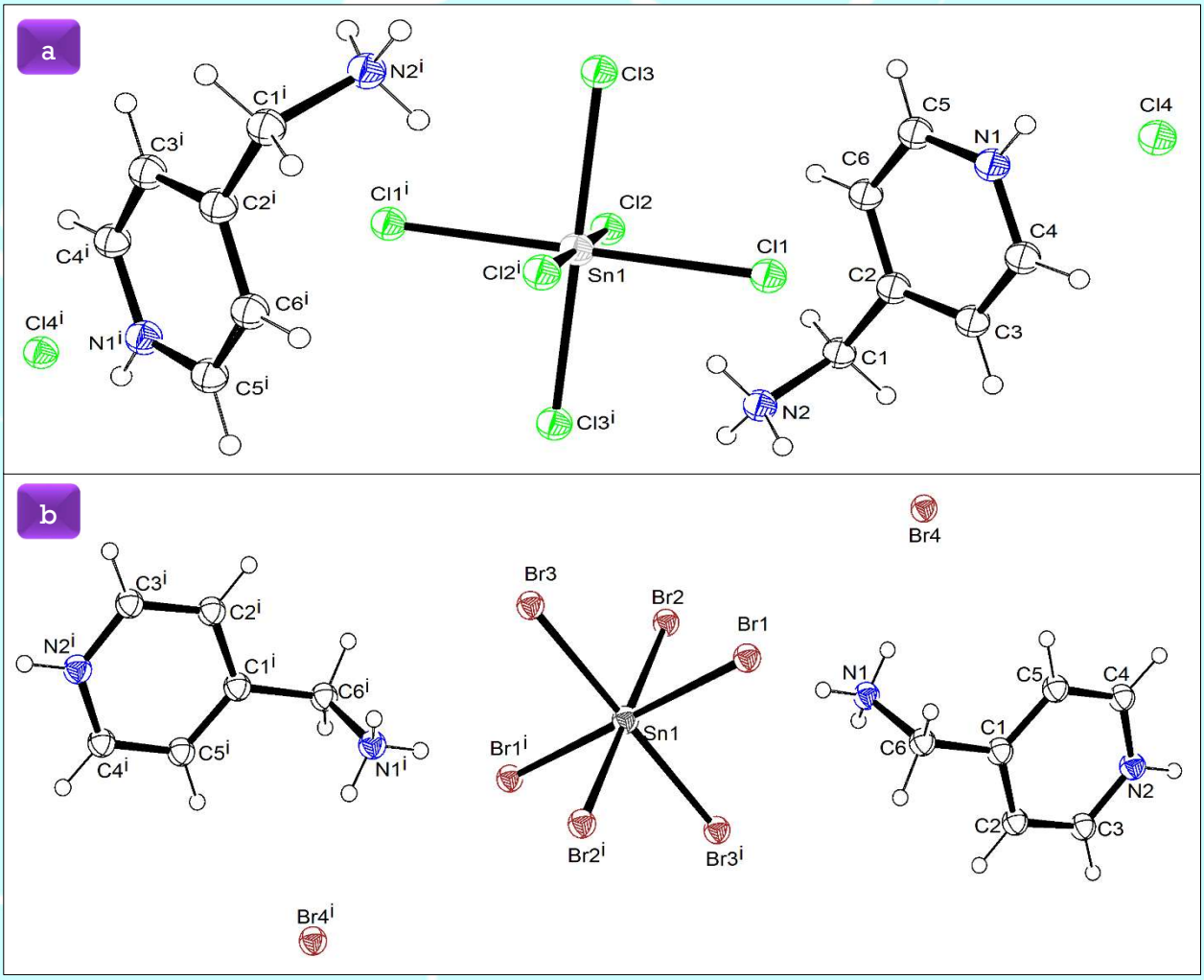


Fig. 2 Displacement ellipsoid plot (35% probability level) of (a) (1) and (b)

ISSN 3030-3907

The asymmetric unit of compound (2) consists of a single diprotonated cation, one bromide ion, and half of a hexabromostannate(IV) anion. These components are intricately connected through a network of hydrogen bonds, specifically N-H•••Br interactions. The cation donates two protons that form strong hydrogen bonds with the bromide ion, creating a robust network of intermolecular interactions. These hydrogen bonds stabilize the structure and influence the packing and arrangement of ions within the crystal lattice. In the crystal structure, the Sn-Cl bond distances range from 2.5908(4) Å to 2.6194(5) Å, indicating a uniform bonding environment around the tin atom. The Br-Sn-Br bond angles vary between 87.344(14)° and 92.657(14)°, reflecting slight deviations from ideal octahedral geometry. The compound exhibits extensive hydrogen-bonding interactions, significantly contributing to its stability and structural organization. The Sn atom is six-coordinated, forming a quasi-regular octahedral arrangement. This coordination geometry is stabilized by the surrounding chloride ions, which, along with the hydrogen bonds, create a robust three-dimensional network within the crystal lattice. The nearly regular octahedral configuration of the $SnBr_6^{2-}$ anion, combined with the extensive hydrogen bonding, highlights the intricate balance of forces that define the structural characteristics of this compound. Table 2 details the polyhedral properties of compound (2), specifically focusing on the $SnBr_6^{2-}$ anion. This anion exhibits octahedral coordination geometry, as illustrated in Fig. S2(b). The bond angle variance is measured at 2.9376°, indicating only minor deviations from the ideal octahedral angles of 90°. Furthermore, the effective coordination number is calculated to be 5.9950, which is nearly perfect compared to the ideal value of 6. These measurements collectively demonstrate that the $SnBr_6^{2-}$ anion maintains nearly perfect octahedral geometry. The minimal bond angle variance suggests a highly symmetrical and stable coordination environment around the tin atom. The hydrogen bonds present in compound (2) are detailed in Table 3 and illustrated in Fig. 3(b). Notably, the hydrogen atom H(1B) participates in bifurcated hydrogen bonding interactions with two bromine atoms. These interactions include N(2)•••Br(1) and N(2)•••Br(2) with corresponding distances of 3.540(4) Å and 3.703(4) Å, respectively. This intricate hydrogen bonding network significantly contributes to the stability and structural integrity of the compound. The centroid-centroid contact distance between adjacent aromatic rings is 3.664 Å, with an interplanar angle of 21.88°. This stacking arrangement exhibits the characteristics of slipped stacking alignment. The horizontal displacement of the rings, or the offset, ranges from 1.339 Å to 1.388 Å, while the plane-to-plane distance is measured at 3.365 Å (Fig. 4(b)). This offset stacking arrangement indicates a significant π-π interaction, which contributes to the overall stability and

ISSN 3030-3907

structural cohesion of the crystal lattice. Both the compounds are isostructural with small variations in lattice parameters.

Table 1.

Crystal data and structure refinement for (1) and (2).

CCDC	2333700	2333701
Empirical formula	$C_{12}H_{20}Cl_8N_4Sn$	$C_{12}H_{20}Br_8N_4Sn$
Formula weight (g/mol)	622.61	978.29
Temperature (K)	294(2)	100(2)
Wavelength (Å)	0.71073	0.71073
Crystal system	Triclinic	Triclinic
Space group	Pī	Pī
a, b, c (Å)	7.1673(6), 7.3639(6), 11.0556(9)	7.3010(3), 7.5683(4), 11.3687(6)
α, β, γ (°)	83.368(3), 83.660(3), 74.919(3)	83.478(2), 84.939(2), 74.221(2)
Volume (A^3)	557.67(8)	599.53(5)
Z	1	1
Density (calculated) (g/cm^{-3})	1.854	2.710
Absorption coefficient (mm^{-1})	2.109	14.401
F(000)	306	450
Crystal size (mm^3)	0.18 x 0.14 x 0.10	0.209 x 0.122 x 0.055
Theta range for data collection	2.954 to 30.617°	3.195 to 27.487°
Index ranges	-10≤ h≤10, -10≤k ≤10, -15≤l≤15	-9 ≤ h ≤ 9, -9 ≤ k ≤ 9, -14 ≤ l ≤ 14
Reflections collected	3748	21604
Independent reflections	3410 [R(int) = 0.0212]	2734 [R(int) = 0.0572]
Absorption correction	Multi-scan	Semi-empirical from equivalents

ISSN 3030-3907

Max. and min. transmission	0.7461 and 0.6263	0.4917 and 0.2194
Refinement method	Full-matrix least-squares on F^2	Full-matrix least-squares on F^2
Data / restraints / parameters	3410 / 4 / 130	2734 / 6 / 127
Goodness-of-fit on F^2	1.067	1.084
Final R indices [I>2sigma(I)]	R1 = 0.0211, wR2 = 0.0505	R1 = 0.0315, wR2 = 0.0868
R indices (all data)	R1 = 0.0229, wR2 = 0.0522	R1 = 0.0358, wR2 = 0.0916
Extinction coefficient	n/a	n/a
Largest diff. peak and hole ($e.Å^{-3}$)	0.946 and -0.729	1.250 and -1.632

Table 2

Polyhedral parameters for compounds (1) and (2).

	(1)		(2)
	Bond distance (Å)		**Bond distance (Å)**
Sn(1)-Cl(1)	2.4398(5)	Sn(1)-Br(1)	2.6194(5)
Sn(1)-Cl(1)^i	2.4398(5)	Sn(1)-Br(1)^i	2.6194(5)
Sn(1)-Cl(2)	2.4292(6)	Sn(1)-Br(2)	2.5935(6)
Sn(1)-Cl(2)^i	2.4292(6)	Sn(1)-Br(2)^i	2.5935(6)
Sn(1)-Cl(3)	2.4176(5)	Sn(1)-Br(3)	2.5908(5)
Sn(1)-Cl(3)^i	2.4176(5)	Sn(1)-Br(3)^i	2.5908(5)
Average bond length (Å)	2.4288		2.6012
Polyhedral volume ($Å^3$)	19.0806		23.4379
Distortion index (bond length)	0.00309		0.00466
Quadratic elongation	1.0009		1.0009
Bond angle variance ($deg.^2$)	2.9569		2.9376
Effective coordination number	5.9972		5.9950

ISSN 3030-3907

3.3. Bond valence sum (BVS) analysis

BVS analysis determines the valence of the central atom using experimentally derived bond distances, indirectly verifying crystal structures. It relies on the R_{ij} value for an i–j bond, typically ionic [23-26]. The oxidation state of a central atom 'i' matches the bond valence, V, with the total valence being its oxidation state, calculated by $V = \Sigma v_{ij} = \exp[(R_o–R_{ij})/b]$, where R_o is a reported value for many ionic compounds [27], R_{ij} is the bond distance, and b is a constant (assumed as 0.37) [28]. The BVS of (1) and (2) are 3.97 and 3.93, respectively (Table 4), confirming the tin's formal oxidation state as 4+ definitively.

Table 3

Hydrogen bonds for (1) and (2) [Å and °].

D-H•••A	d(D-H)	d(H•••A)	d(D•••A)	<(DHA)
(1)				
N(1)-H(1)•••Cl(4)	0.86(1)	2.49(2)	3.165(2)	136(2)
N(1)-H(1)•••Cl(4)	0.86(1)	2.57(2)	3.208(1)	132(2)
N(2)-H(2A)•••Cl(1)	0.88(2)	2.75(2)	3.477(4)	140(2)
N(2)-H(2A)•••Cl(2)	0.88(2)	2.89(2)	3.575(1)	136(2)
N(2)-H(2A)•••Cl(3)	0.88(2)	2.69(2)	3.324(2)	129(2)
N(2)-H(2B)•••Cl(2)	0.90(2)	2.43(2)	3.305(2)	165(2)
N(2)-H(2C)•••Cl(4)	0.89(3)	2.20(3)	3.080(2)	168(3)
C(4)-H(4)•••Cl(1)	0.93	2.922	3.706(2)	142.9
C(5)-H(5)•••Cl(4)	0.93	2.8457	3.361(2)	116.1
C(6)-H(6)•••Cl(3)	0.93	2.7567	3.651(2)	161.5
(2)				
C(2)-H(2)•••Br(3)#1	0.95	2.84	3.771(5)	165.9
C(3)-H(3)•••Br(2)#2	0.95	3.05	3.759(5)	132.9
C(3)-H(3)•••Br(4)#2	0.95	2.94	3.481(5)	117.8
C(4)-H(4)•••Br(1)#3	0.95	3.00	3.809(5)	143.3
C(4)-H(4)•••Br(4)#4	0.95	2.92	3.471(5)	117.9
C(5)-H(5)•••Br(4)	0.95	3.07	3.717(5)	126.8
C(6)-H(6A)•••Br(4)#3	0.99	3.08	3.940(5)	146.6
N(2)-H(2A)•••Br(4)#2	0.88	2.66	3.335(4)	134.6
N(2)-H(2A)•••Br(4)#4	0.88	2.65	3.327(4)	134.7
N(1)-H(1A)•••Br(2)#5	0.858(18)	2.58(2)	3.411(4)	164(4)

ISSN 3030-3907

N(1)-H(1B)•••Br(1)	0.854(18)	2.80(3)	3.540(4)	146(5)
N(1)-H(1B)•••Br(2)	0.854(18)	3.05(5)	3.703(4)	135(5)
N(1)-H(1C)•••Br(4)	0.850(19)	2.40(2)	3.227(4)	164(5)

Symmetry transformations used to generate equivalent atoms:

#1 -x+2,-y+1,-z+1 #2 x+1,y-1,z, #3 -x+1,-y+1,-z+2 #4 -x+1,-y,-z+2 #5 -x+1,-y+1,-z+1

REFERENCES

1. F. Hao, C.C. Stoumpos, R.P.H. Chang, M.G. Kanatzidis, Anomalous band gap behavior in mixed Sn and Pb perovskites enables broadening of absorption spectrum in solar cells, J. Am. Chem. Soc. 136 (2014) 8094-8099.

2. C.C. Stoumpos, C.D. Malliakas, M.G. Kanatzidis, Semiconducting tin and lead iodide perovskites with organic cations: phase transitions, high mobilities, and near-infrared photoluminescent properties, Inorg. Chem. 52 (2013) 9019-9038.

3. W.-Q. Liao, Y. Zhang, C.-L. Hu, J.-G. Mao, H.-Y. Ye, P.-F. Li, S.D. Huang, R.-G. Xiong, A lead-halide perovskite molecular ferroelectric semiconductor, Nat. Commun. 6 (1) (2015) 1-7.

4. C. Kim, T.D. Huan, S. Krishnan, R. Ramprasad, Data descriptor: a hybrid organic-inorganic perovskite dataset, Sci. Data 4 (2017) 1–11 170057.

5. H. Yuping, G. Galli, Perovskites for Solar Thermoelectric Applications: A First Principle Study of $CH_3NH_3AI_3$ (A = Pb and Sn), Chem. Mater. 26 (2014) 5394-5400.

6. A. Kojima, K. Teshima, Y. Shirai, T. Miyasaka, Organometal halide perovskites as visible-light sensitizers for photovoltaic cells, J. Am. Chem. Soc. 131 (2009) 6050–6051.

7. X. Shan, J. Li, M. Chen, T. Geske, S. Ganesh, R. Bade, Junction propagation in organometal halide perovskite-polymer composite thin films, Y. Zhibin, J. Phys. Chem. Lett. 8 (2017) 2412–2419.

8. M. Manonmani, C. Balakrishnan, M. Dhanalakshmi, S.R. Ahamed, G. Vinitha, R.M. Sockalingam, Synthesis, structure, third-order nonlinear optical properties and Hirshfeld surface analysis of tetrakis (azepanium) hexachlorostannate(IV) dichloride and tetrakis (azepanium) hexabromostannate (IV) dibromide, J. Mol. Struct. 1227 (2021) 129515.

9. K. Ramalingam, T. Rajaraman, Structure-bandgap tunability of metal halide perovskites: Synthesis, spectral, single crystal X-ray structural, BVS, CShM and Hirshfeld surface analysis of piperidinium hexahalostannates(IV), J. Mol. Struct., 1273 (2023) 134285.

10. Y. Zhao, K. Zhu, Organic-inorganic hybrid lead halide perovskites for optoelectronic and electronic applications, Chem. Soc. Rev. 45 (2016) 655–689.

ISSN 3030-3907

11. L. Lanzetta, J.M. Marin-Beloqui, I. Sanchez-Molina, D. Ding, S.S. Haque, Two-dimensional organic tin halide perovskites with tunable visible emission and their use in light-emitting devices, ACS Energy Lett. 2 (2017) 1662–1668.
12. K. Ramalingam, T. Rajaraman, Metal-organic hybrids of tin (IV) with tuneable band gap: Synthesis, spectral, single crystal X-ray structural, BVS and CSM analysis of morpholinium hexahalostannate (IV), J. Mol. Struct. 1218 (2020) 128489.
13. X. Liu, P. Long, Z. Sun, Z. Yi, Optical, electrical and photoelectric properties of layered perovskite ferroelectric Bi_2WO_6 crystals, J. Mater. Chem. C 4 (2016) 7563–7570.
14. Z. Lin, Y.N. Wu, S.Y. Xu, B.C. Chen, P.W. Huang, X.H. Qi, Y.P. Lin, K.Z. Du, Dopant effect on the optical and thermal properties of the 2D organic–inorganic hybrid perovskite (HDA)2 PbBr4, Dalton Trans. 53(4) (2024)1691-1697.
15. D. Lencer, M. Salinga, M. Wuttig, Design rules for phase-change materials in data storage applications, Adv. Mater. 23 (2011) 2030–2058.

ISSN 3030-3907